energy range of a detector. The DQE drops significantly if a detector is used out of its energy range. For instance, the energy range of MWPC and microgap detectors is about 3 to 15 keV. The DQE with Cu $K\alpha$ radiation (8.06 keV) is about 80%, but drops gradually when approaching the lower or higher energy limits. The energy range of imaging plates is much wider (4–48 keV). The energy range of a CCD, depending on the phosphor, covers from 5 keV up to the hard X-ray region.

2.5.3.2.4. *Detection limit and dynamic range*

The detection limit is the lowest number of counts that can be distinguished from the absence of true counts within a specified confidence level. The detection limit is estimated from the mean of the noise, the standard deviation of the noise and some confidence factor. In order to have the incoming X-ray photons counted with a reasonable statistical certainty, the counts produced by the X-ray photons should be above the detector background-noise counts.

The dynamic range is defined as the range extending from the detection limit to the maximum count measured in the same length of counting time. The linear dynamic range is the dynamic range within which the maximum counts are collected within the specified linearity. For X-ray detectors, the dynamic range most often refers to linear dynamic range, since only a diffraction pattern collected within the linear dynamic range can be correctly interpreted and analysed. When the detection limit in count rate approaches the noise rate at extended counting time, the dynamic range can be approximated by the ratio of the maximum count rate to the noise rate.

Dynamic range is very often confused with the maximum count rate, but must be distinguished. With a low noise rate, a detector can achieve a dynamic range much higher than its count rate. For example, if a detector has a maximum linear count rate of 10^5 s^{-1} with a noise rate of 10^{-3} s^{-1}, the dynamic range can approach 10^8 for an extended measurement time. The dynamic range for a 2D detector has the same definition as for a point detector, except that with a 2D detector the whole dynamic range extending from the detection limit to the maximum count can be observed from different pixels simultaneously. In order to record the entire two-dimensional diffraction pattern, it is necessary for the dynamic range of the detector to be at least the dynamic range of the diffraction pattern, which is typically in the range 10^2 to 10^6 for most applications. If the range of reflection intensities exceeds the dynamic range of the detector, then the detector will either saturate or have low-intensity patterns truncated. Therefore, it is desirable that the detector has as large a dynamic range as possible.

2.5.3.2.5. *Types of 2D detectors*

2D detectors can be classified into two broad categories: photon-counting detectors and integrating detectors (Lewis, 1994). Photon-counting area detectors can detect a single X-ray photon entering the active area. In a photon-counting detector, each X-ray photon is absorbed and converted to an electrical pulse. The number of pulses counted per unit time is proportional to the incident X-ray flux. Photon-counting detectors typically have high counting efficiency, approaching 100% at low count rate. The most commonly used photon-counting 2D detectors include MWPCs, Si-pixel arrays and microgap detectors. Integrating area detectors, also referred to as analogue X-ray imagers, record the X-ray intensity by measuring the analogue electrical signals converted from the incoming X-ray flux. The signal size of each pixel is proportional to the fluence of incident X-rays. The most commonly used integrating 2D detectors include image plates (IPs) and charge-coupled devices (CCDs).

The selection of an appropriate 2D detector depends on the X-ray diffraction application, the sample condition and the X-ray beam intensity. In addition to geometry features, such as the active area and pixel format, the most important performance characteristics of a detector are its sensitivity, dynamic range, spatial resolution and background noise. The detector type, either photon-counting or integrating, also leads to important differences in performance. Photon-counting 2D detectors typically have high counting efficiency at low count rate, while integrating 2D detectors are not so efficient at low count rate because of the relatively high noise background. An MWPC has a high DQE of about 0.8 when exposed to incoming local fluence from single photons up to about 10^3 photons s^{-1} mm^{-2}. The diffracted X-ray intensities from a polycrystalline or powder sample with a typical laboratory X-ray source fall into this fluence range. This is especially true with microdiffraction, where high sensitivity and low noise are crucial to reveal the weak diffraction pattern. Owing to the counting losses at a high count rate, the DQE of an MWPC decreases with increasing count rate and quickly saturates above 10^3 photons s^{-1} mm^{-2}. Therefore, an MWPC is not suitable for collecting strong diffraction patterns or for use with high intensity sources, such as synchrotron X-ray sources. An IP can be used in a large fluence range from 10 photons s^{-1} mm^{-2} and up with a DQE of 0.2 or lower. An IP is suitable for strong diffraction from single crystals with high-intensity X-ray sources, such as a rotating-anode generator or synchrotron X-ray source. With weak diffraction signals, the image plate cannot resolve the diffraction data near the noise floor. A CCD detector can also be used over a large X-ray fluence range from 10 photons s^{-1} mm^{-2} to very high fluence with a much higher DQE of 0.7 or higher. It is suitable for collecting diffraction of medium to strong intensity from single-crystal or polycrystalline samples. Owing to the relatively high sensitivity and high local count rate, CCDs can be used in systems with either sealed-tube X-ray sources, rotating-anode generators or synchrotron X-ray sources. With a low DQE at low fluence and the presence of dark-current noise, a CCD is not a good choice for applications with weak diffraction signals. A microgap detector has the best combination of high DQE, low noise and high count rate. It has a DQE of about 0.8 at an X-ray fluence from single photons up to about 10^5 photons s^{-1} mm^2. It is suitable for microdiffraction when high sensitivity and low noise are crucial to reveal weak diffraction patterns. It can also handle high X-ray fluence from strong diffraction patterns or be used with high-intensity sources, such as rotating-anode generators or synchrotron X-ray sources.

2.5.3.3. *Data corrections and integration*

2D diffraction patterns contain abundant information. In order to interpret and analyse 2D patterns accurately it is necessary to apply some data-treatment processes (Sulyanov *et al.*, 1994; Scheidegger *et al.*, 2000; Cervellino *et al.*, 2006; Boesecke, 2007; Rowe, 2009). Most data-treatment processes can be categorized as having one of the following four purposes: to eliminate or reduce errors caused by detector defects; to remove undesirable effects of instrument and sample geometry; to transfer a 2D frame into a format such that the data can be presented or further analysed by conventional means and software; and cosmetic treatment, such as smoothing a frame for reports and publications.

2.5.3.3.1. *Nonuniform response correction*

A 2D detector can be considered as an array of point detectors. Each pixel may have its own response, and thus a 2D detector may exhibit some nonuniformity in intensity measurement when exposed to an isotropic source. The nonuniform response can be caused by manufacturing defects, inadequate design or limitations of the detector technology. For instance, a nonuniform phosphor screen or coupling fibre optic for a CCD detector may cause nonuniformity in quantum efficiency (Tate *et al.*, 1995). A gas-filled detector may have a different intensity response between the detector edge and centre due to the variation in the electric field from the centre to the edge. A thorough correction to the nonuniformity of the intensity response can be performed if the detector counting curves of all pixels are given. In practice, this is extremely difficult or impossible, because the behaviour of a pixel may be affected by the condition of the adjacent pixels and the whole detector. The practical way to correct the nonuniformity of the intensity response is to collect an X-ray image from an isotropic point source at the instrument centre and use the image data frame to generate a correction table for the future diffraction frames. The frame collected with the isotropic source is commonly referred to as a 'flood-field' frame or a flat-field image, and the correction is also called a flood-field correction or flat-field correction (Stanton *et al.*, 1992). Another type of correction for a nonuniform response is background correction. Background correction is done by subtracting a background frame from the data frame. The background frame is collected without X-ray exposure. Integrating detectors, such as image plates or CCDs, have a strong background which must be considered in nonuniform response correction. Photon-counting detectors, such as MWPC and microgap detectors, have negligible background, so background correction is not necessary.

The X-ray source for calibration for flood-field correction should be a uniform, spherically radiating point source. Identical brightness should be observed at any pixel on the detector. The radiation strength of the source should match the intensity of the diffraction data to be collected. The photon energy of the source should be the same as or close to the X-ray beam used for diffraction-data collection so that the detector behaves the same way during calibration and data collection.

There are many choices of calibration sources, including X-ray tubes, radioactive sources, diffuse scattering or X-ray fluorescence. The radioactive source Fe-55 (^{55}Fe) is the most commonly used calibration source for a diffraction system because of its major photon energy level of 5.9 keV. X-ray fluorescence is an alternative to a radioactive source. Fluorescence emission is generated by placing a fluorescent material into the X-ray beam. Fluorescence radiation is an isotopic point source if the irradiated area is a small point-like area. For example, Cu $K\alpha$ can produce intense fluorescence from materials containing significant amounts of iron or cobalt and Mo $K\alpha$ can produce intense fluorescence from materials containing yttrium. In order to avoid a high localized intensity contribution from X-ray diffraction, the fluorescent material should be amorphous, such as a glassy iron foil. An alternative to a glassy alloy foil is amorphous lithium borate glass doped with the selected fluorescent element up to a 10% concentration (Moy *et al.*, 1996).

There are many algorithms available for flood-field correction depending on the nature of the 2D detector. The correction is based on the flood-field frame collected from the calibration source. The simplest flood-field correction is to normalize the counts of all pixels to the same level assuming that all pixels have the same response curve. The corrected frame from an isotropic source is not flat, but maintains the $\cos^3 \phi$ falloff effect, which will be considered in the frame integration. For gas-filled detectors, such as MWPC and microgap detectors, the pixel intensity response is not independent, but is affected by X-ray exposure to surrounding pixels and the whole detector. Flood-field correction is carried out by applying a normalization factor to each pixel in which a 'rubber-sheet' kind of stretching and shrinking in regions along the x and y detector axes slightly alters the size of each pixel (He, 2009). The total number of counts remains the same after the correction but is redistributed throughout the pixels so that the image from an isotropic source is uniformly distributed across the detector. The flood-field calibration must be done with the same sample-to-detector distance as for the diffraction-data collection.

2.5.3.3.2. *Spatial correction*

In an ideal flat 2D detector, not only does each pixel have the same intensity response, but also an accurate position. The pixels are aligned in the x and y directions with equal spacing. In most cases we assume that the detective area is completely filled by pixels, so the distance between two neighbouring pixels is equivalent to the pixel size. The deviation from this perfect pixel array is called spatial distortion. The extent of spatial distortion is dependent on the nature and limitation of the detector technology. A CCD detector with 1:1 demagnification may have a negligible spatial distortion, but the barrel distortion in the coupling fibre-optic taper can introduce substantial spatial distortion. An image-plate system may have spatial distortion caused by imperfections in the scanning system (Campbell *et al.*, 1995). MWPC detectors typically exhibit more severe spatial distortion due to the window curvature and imperfections in the wire anode (Derewenda & Helliwell, 1989).

The spatial distortion is measured from X-ray images collected with a uniformly radiating point source positioned at the instrument centre and a fiducial plate fastened to the front surface of the detector. The source for spatial correction should have a very accurate position, point-like shape and small size. The fiducial plate is a metal plate with accurately distributed pinholes in the x and y directions. The X-ray image collected with this setup contains sharp peaks corresponding to the pinhole pattern of the fiducial plate. Since accurate positions of the peaks are given by the fiducial plate, the spatially corrected image is a projection of the collected image to this plane. Therefore, the detector plane is defined as the contacting plane between the fiducial plate and detector front face.

Spatial correction restores the spatially distorted diffraction frame into a frame with correct pixel positions. Many algorithms have been suggested for spatial correction (Sulyanov *et al.*, 1994; Tate *et al.*, 1995; Stanton *et al.*, 1992; Campbell *et al.*, 1995). In the spatially corrected frame each pixel is generated by computing the pixel count from the corresponding pixels based on a spatial-correction look-up table. In a typical spatial-correction process, an image containing the spots from the calibration source passing through the fiducial plate is collected. The distortion of the image is revealed by the fiducial spots. Based on the known positions of the corresponding pinholes in the fiducial plate, the distortion of each fiducial spot can be determined. The spatial correction for all pixels can be calculated and stored as a look-up table. Assuming that the detector behaves the same way in the real diffraction-data collection, the look-up table generated from the fiducial image can then be applied to the real diffraction frames.

The spatial calibration must be done at the same sample-to-detector distance as the diffraction-data collection.

2.5.3.3.3. *Frame integration*

2D frame integration is a data-reduction process which converts a two-dimensional frame into a one-dimensional intensity profile. Two forms of integration are generally of interest in the analysis of a 2D diffraction frame from polycrystalline materials: γ integration and 2θ integration. γ integration sums the counts in 2θ steps ($\Delta 2\theta$) along constant 2θ conic lines and between two constant γ values. γ integration produces a data set with intensity as a function of 2θ. 2θ integration sums the counts in γ steps ($\Delta\gamma$) along constant γ lines and between two constant 2θ conic lines. 2θ integration produces a data set with intensity as a function of γ. γ integration may also be carried out with the integration range in the vertical direction as a constant number of pixels. This type of γ integration may also be referred to as slice integration. A diffraction profile analogous to the conventional diffraction result can be obtained by either γ integration or slice integration over a selected 2θ range. Phase ID can then be done with conventional search/match methods. 2θ integration is of interest for evaluating the intensity variation along γ angles, such as for texture analysis, and is discussed in more depth in Chapter 5.3.

The γ integration can be expressed as

$$I(2\theta) = \int_{\gamma_1}^{\gamma_2} J(2\theta, \gamma)\, \mathrm{d}\gamma, \quad 2\theta_1 \leq 2\theta \leq 2\theta_2, \tag{2.5.23}$$

where $J(2\theta, \gamma)$ represents the two-dimensional intensity distribution in the 2D frame and $I(2\theta)$ is the integration result as a function of intensity *versus* 2θ. γ_1 and γ_2 are the lower limit and upper limit of integration, respectively, which are constants for γ integration. Fig. 2.5.13 shows a 2D diffraction frame collected from corundum (α-Al_2O_3) powder. The 2θ range is from 20 to 60° and the 2θ integration step size is 0.05°. The γ-integration range is from 60 to 120°. In order to reduce or eliminate the dependence of the integrated intensity on the integration interval, the integrated value at each 2θ step is normalized by the number of pixels, the arc length or the solid angle. γ integration with normalization by the solid angle can be expressed as

$$I(2\theta) = \frac{\int_{\gamma_1}^{\gamma_2} J(2\theta, \gamma)(\Delta 2\theta)\, \mathrm{d}\gamma}{\int_{\gamma_1}^{\gamma_2} (\Delta 2\theta)\, \mathrm{d}\gamma}, \quad 2\theta_1 \leq 2\theta \leq 2\theta_2. \tag{2.5.24}$$

Since the $\Delta 2\theta$ step is a constant, the above equation becomes

$$I(2\theta) = \frac{\int_{\gamma_1}^{\gamma_2} J(2\theta, \gamma)\, \mathrm{d}\gamma}{\gamma_2 - \gamma_1}, \quad 2\theta_1 \leq 2\theta \leq 2\theta_2. \tag{2.5.25}$$

There are many integration software packages and algorithms available for reducing 2D frames into 1D diffraction patterns for polycrystalline materials (Cervellino *et al.*, 2006; Rodriguez-Navarro, 2006; Boesecke, 2007). With the availability of tremendous computer power today, a relatively new method is the bin method, which treats pixels as having a continuous distribution in the detector. It demands more computer power than older methods, but delivers much more accurate and smoother results even with $\Delta 2\theta$ integration steps significantly smaller than the pixel size. Depending on the relative size of $\Delta 2\theta$ to the pixel size, each contributing pixel is divided into several 2θ 'bins'. The intensity counts of all pixels within the $\Delta 2\theta$ step are summarized. All the normalization methods in the above integration, either by pixel, arc or solid angle, result in an intensity level of one pixel or unit solid angle. Since a pixel is much smaller than the active area of a typical point detector, the normalized integration tends to result in a diffraction pattern with fictitiously low intensity counts, even though the true counts in the corresponding $\Delta 2\theta$ range are significantly higher. In order to avoid this misleading outcome, it is reasonable to introduce a scaling factor. However, there is no accurate formula for making the integrated profile from a 2D frame comparable to that from a conventional point-detector scan. The best practice is to be aware of the differences and to try not to make direct comparisons purely based on misleading intensity levels. Generally speaking, for the same exposure time, the total counting statistics from a 2D detector are significantly better than from a 0D or 1D detector.

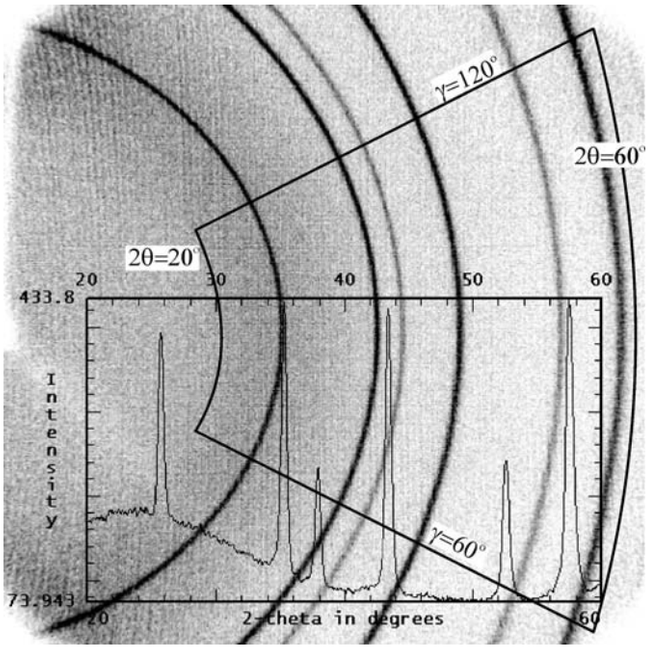

Figure 2.5.13
A 2D frame showing γ integration.

2.5.3.3.4. *Lorentz, polarization and absorption corrections*

Lorentz and polarization corrections may be applied to the diffraction frame to remove their effect on the relative intensities of Bragg peaks and background. The 2θ angular dependence of the relative intensity is commonly given as a Lorentz–polarization factor, which is a combination of Lorentz and polarization factors. In 2D diffraction, the polarization factor is a function of both 2θ and γ, therefore it should be treated in the 2D frames, while the Lorentz factor is a function of 2θ only. The Lorentz correction can be done either on the 2D frames or on the integrated profile. In order to obtain relative intensities equivalent to a conventional diffractometer with a point detector, reverse Lorentz and polarization corrections may be applied to the frame or integrated profile.

The Lorentz factor is the same as for a conventional diffractometer. For a sample with a completely random orientation distribution of crystallites, the Lorentz factor is given as

$$L = \frac{\cos\theta}{\sin^2 2\theta} = \frac{1}{4\sin^2\theta\cos\theta}. \tag{2.5.26}$$

The Lorentz factor may be given by a different equation for a different diffraction geometry (Klug & Alexander, 1974). The forward and reverse Lorentz corrections are exactly reciprocal

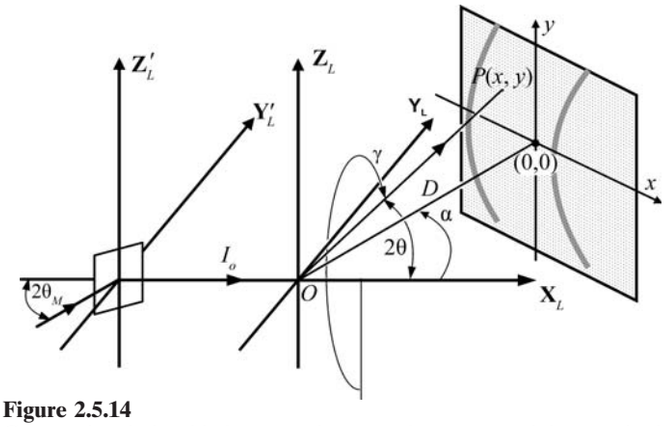

Figure 2.5.14
Geometric relationship between the monochromator and detector in the laboratory coordinates.

and effectively cancel each other. Therefore, it is not necessary to perform the Lorentz correction to the frame before integration if relative intensities equivalent to a conventional Bragg–Brentano diffractometer are expected. The Lorentz correction can be done on the integrated diffraction profiles in the same way as on the diffraction profiles collected with conventional diffractometers.

When a non-polarized X-ray beam is scattered by matter, the scattered X-rays are polarized. The intensity of the diffracted beam is affected by the polarization; this effect is expressed by the polarization factor. In two-dimensional X-ray diffraction the diffraction vectors of the monochromator diffraction and sample crystal diffraction are not necessarily in the same plane or perpendicular planes. Therefore, the overall polarization factor is a function of both 2θ and γ. Fig. 2.5.14 illustrates the geometric relationship between the monochromator and detector in the laboratory coordinates, X_L, Y_L, Z_L. The monochromator is located at the coordinates X_L, Y'_L, Z'_L, which is a translation of the laboratory coordinates along the X_L axis in the negative direction. The monochromator crystal is rotated about the Z'_L axis and $2\theta_M$ is the Bragg angle of the monochromator crystal. The diffracted beam from the monochromator propagates along the X_L direction. This is the incident beam to the sample located at the instrument centre O. The 2D detector location is given by the sample-to-detector distance D and swing angle α. The pixel $P(x, y)$ represents an arbitrary pixel on the detector. 2θ and γ are the corresponding diffraction-space parameters for the pixel. Since a monochromator or other beam-conditioning optics can only be used on the incident beam, the polarization factor for 2D-XRD can then be given as a function of both θ and γ:

$$P(\theta, \gamma) = \frac{(1 + \cos^2 2\theta_M \cos^2 2\theta)\sin^2\gamma + (\cos^2 2\theta_M + \cos^2 2\theta)\cos^2\gamma}{1 + \cos^2 2\theta_M}. \quad (2.5.27)$$

If the crystal monochromator rotates about the Y'_L axis, *i.e.* the incident plane is perpendicular to the diffractometer plane, the polarization factor for two-dimensional X-ray diffraction can be given as

$$P(\theta, \gamma) = \frac{(1 + \cos^2 2\theta_M \cos^2 2\theta)\cos^2\gamma + (\cos^2 2\theta_M + \cos^2 2\theta)\sin^2\gamma}{1 + \cos^2 2\theta_M}. \quad (2.5.28)$$

In the above equations, the term $\cos^2 2\theta_M$ can be replaced by $\left|\cos^n 2\theta_M\right|$ for different monochromator crystals. For a mosaic crystal, such as a graphite crystal, $n = 2$. For most real monochromator crystals, the exponent n takes a value between 1 and 2. For near perfect monochromator crystals, n approaches 1 (Kerr & Ashmore, 1974). All the above equations for polarization factors may apply to multilayer optics. However, since multilayer optics have very low Bragg angles, $\left|\cos^n 2\theta_M\right|$ approximates to unity. The γ dependence of the polarization factor diminishes in this case. The polarization factor approaches

$$P(\theta, \gamma) \simeq \frac{1 + \cos^2 2\theta}{2}. \quad (2.5.29)$$

2.5.3.3.5. *Air scatter*

X-rays are scattered by air molecules in the beam path between the X-ray source and detector. Air scatter results in two effects: one is the attenuation of the X-ray intensity, the other is added background in the diffraction pattern. Air scatter within the enclosed primary beam path – for instance, in the mirror, monochromator housing or collimator – results in attenuation of only the incident beam. The enclosed beam path can be purged by helium gas or kept in vacuum to reduce the attenuation so that no correction is necessary for this part of the air scatter. The open beam between the tip of the collimator and the sample generates an air-scatter background pattern, which is the major part of the air scatter. In the secondary beam path, the air scatter from the diffracted beam may generate background too, but the main effect of the air scatter is inhomogeneous attenuation of the diffraction pattern due to the different beam path lengths between the centre and the edge of the detector.

The background generated by air scattering from the open incident-beam path has a strong 2θ dependence. The specific scattering curve depends on the length of the open primary beam path, the beam size and the wavelength of the incident beam. There are two approaches to correct air scatter. One is to collect an air-scatter background frame under the same conditions as the diffraction frame except without a sample. The background frame is then subtracted from the diffraction frame. Another approach is to remove the background from the integrated profile, since the background is 2θ dependent.

The attenuation of the diffracted beam by air absorption depends on the distance between the sample and pixel. For a flat detector, air absorption can be corrected by

$$p_c(x, y) = p_o(x, y)\exp\left[\mu_{\text{air}}(D^2 + x^2 + y^2)^{1/2}\right], \quad (2.5.30)$$

where $p_o(x, y)$ is the original pixel intensity of the pixel $P(x, y)$ and $p_c(x, y)$ is the corrected intensity. The detector centre is given by (0, 0). μ_{air} is the linear absorption coefficient of air. The value of μ_{air} is determined by the radiation wavelength. By approximation, for air with 80% N_2 and 20% O_2 at sea level and at 293 K, $\mu_{\text{air}} = 0.01\ \text{cm}^{-1}$ for Cu $K\alpha$ radiation. Air scatter and absorption increases with increasing wavelength. For example, $\mu_{\text{air}} = 0.015\ \text{cm}^{-1}$ for Co $K\alpha$ radiation and $0.032\ \text{cm}^{-1}$ for Cr $K\alpha$ radiation. The absorption coefficient for Mo $K\alpha$ radiation, $\mu_{\text{air}} = 0.001\ \text{cm}^{-1}$, is only one-tenth of that for Cu $K\alpha$ radiation, so an air-absorption correction is not necessary. Alternatively, the absorption correction may be normalized to the absorption level in the beam centre as

$$p_c(x, y) = p_o(x, y)\exp\left\{\mu_{\text{air}}\left[(D^2 + x^2 + y^2)^{1/2} - D\right]\right\}. \quad (2.5.31)$$

In this normalized correction the attenuation by air scatter is not fully corrected for each pixel, but rather corrected to the same attenuation level as the pixel in the detector centre. This means that the effect of path-length differences between the detector centre pixel and other pixels are eliminated.

2.5.3.3.6. *Sample absorption*

The absorption of X-rays by the sample reduces the diffracted intensity. Many approaches are used to calculate and correct the absorption effect for various sample shapes and geometries [*International Tables for Crystallography* Volume C, Chapter 6.3 (Maslen, 1992); Ross, 1992; Pitschke *et al.*, 1996; Zuev, 2006]. The sample absorption can be measured by the transmission coefficient (also referred to as the absorption factor):

$$A = (1/V) \int_V \exp(-\mu\tau)\, \mathrm{d}V, \tag{2.5.32}$$

where A is the transmission coefficient, μ is the linear absorption coefficient and τ is the total beam path in the sample, which includes the incident-beam path and diffracted-beam path. Fig. 2.5.15(a) shows reflection-mode diffraction with a flat-plate sample. The thickness of the plate is t. z is the distance of the element dV from the sample surface. The normal to the reflection surface is **n**. The incident beam is represented by the unit vector $\mathbf{s}_o$ and the diffracted beam by the unit vector **s**. The transmission coefficient is given as (Maslen, 1992)

$$A = \frac{1 - \exp\{-\mu t[(1/\cos\eta) + (1/\cos\zeta)]\}}{\mu[(\cos\zeta/\cos\eta) + 1]}, \tag{2.5.33}$$

where η is the angle between the incident beam and the normal to the sample surface, and ζ is the angle between the diffracted beam and the sample normal. For two-dimensional X-ray diffraction, there is a single incident-beam direction at a time, but various diffracted-beam directions simultaneously, so

$$\cos\eta = \sin\omega\cos\psi \tag{2.5.34}$$

and

$$\cos\zeta = -\cos 2\theta \sin\omega\cos\psi - \sin 2\theta \sin\gamma\cos\omega\cos\psi - \sin 2\theta\cos\gamma\sin\psi. \tag{2.5.35}$$

The transmission coefficient from equation (2.5.33) contains a length unit, which creates ambiguity if such transmission coefficients are used to correct the intensity pixel-by-pixel. In order to make the relative intensity comparable to the results from Bragg–Brentano geometry, we introduce a new transmission coefficient, which is normalized by the transmission coefficient of the Bragg–Brentano geometry, $A_{\rm BB} = 1/(2\mu)$. This normalized transmission coefficient is also a numerical factor without units. The transmission coefficient with normalization will be denoted by T hereafter in this chapter. The transmission coefficient for reflection-mode diffraction with a flat sample of thickness t is then given as

$$T = A/A_{\rm BB} = \frac{2\cos\eta\big(1 - \exp\{-\mu t[(1/\cos\eta) + (1/\cos\zeta)]\}\big)}{\cos\eta + \cos\zeta}. \tag{2.5.36}$$

For a thick plate or material with a very high linear absorption coefficient, the transmission through the sample thickness is negligible and the above equation becomes

$$T = \frac{2\cos\eta}{\cos\eta + \cos\zeta}. \tag{2.5.37}$$

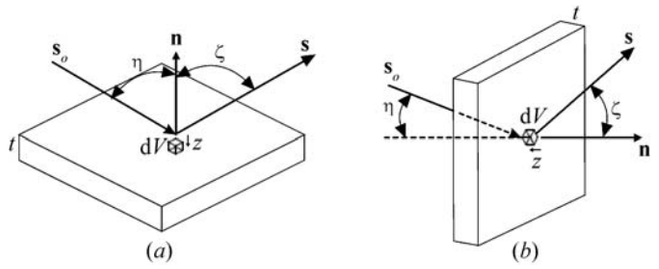

Figure 2.5.15
Absorption correction for a flat slab: (a) reflection; (b) transmission.

Fig. 2.5.15(b) shows transmission-mode diffraction with a flat-plate sample. The thickness of the plate is t. The normal to the reflection surface is represented by the unit vector **n**. The incident beam is represented by the unit vector $\mathbf{s}_o$ and the diffracted beam by the unit vector **s**. η is the angle between the incident beam and the normal of the sample surface, and ζ is the angle between the diffracted beam and the sample normal.

The transmission coefficient normalized by $A_{\rm BB} = 1/(2\mu)$ is given by (Maslen, 1992; Ross, 1992)

$$T = \frac{2\sec\eta[\exp(-\mu t\sec\eta) - \exp(-\mu t\sec\zeta)]}{\sec\zeta - \sec\eta} \quad \text{for } \sec\zeta \neq \sec\eta. \tag{2.5.38}$$

For two-dimensional X-ray diffraction in transmission mode

$$\cos\eta = \sin\omega\sin\psi\sin\varphi + \cos\omega\cos\varphi \tag{2.5.39}$$

and

$$\cos\zeta = (\sin\omega\sin\psi\sin\varphi + \cos\omega\cos\varphi)\cos 2\theta + (\cos\omega\sin\psi\sin\varphi - \sin\omega\cos\varphi)\sin 2\theta\sin\gamma - \cos\psi\sin\varphi\sin 2\theta\cos\gamma. \tag{2.5.40}$$

It is very common practice to set the incident angle perpendicular to the sample surface, *i.e.* $\eta = 0$. For most transmission-mode data collection, equation (2.5.40) becomes

$$T = \frac{2[\exp(-\mu t) - \exp(-\mu t\sec\zeta)]}{\sec\zeta - 1}. \tag{2.5.41}$$

When $\eta = \zeta$, both the numerator and denominator approach zero, and the transmission coefficient should be given by

$$T = 2\mu t\sec\zeta\exp(-\mu t\sec\zeta). \tag{2.5.42}$$

It is common practice to load the sample perpendicular to the incident X-ray beam at the goniometer angles $\omega = \psi = \varphi = 0$. Therefore, $\cos\eta = 1$ and $\cos\zeta = \cos 2\theta$, and the transmission coefficient becomes

$$T = \frac{2\cos 2\theta[\exp(-\mu t) - \exp(-\mu t/\cos 2\theta)]}{1 - \cos 2\theta}. \tag{2.5.43}$$

The maximum scattered intensity occurs when

$$t = \frac{\cos 2\theta\ln\cos 2\theta}{\mu(\cos 2\theta - 1)}. \tag{2.5.44}$$

This equation can be used to select the optimum sample thickness for transmission-mode diffraction. For example, if the measurement 2θ range is between 3 and 50°, the preferred sample thickness should be given by μt = 0.8–1.0.

references